International Journal on Recent and Innovation Trends in Computing and Communication
ISSN: 2321-8169 Volume: 11 Issue: 9
***Article Received:** 25 July 2023 **Revised:** 12 September 2023 **Accepted:** 30 September 2023*

Prediction of Covid-19 Multiparametric Biomarkers and Drug Target of Patients for Risk Stratification Using Machine Learning Approach

Jagannath Jijaba Kadam[1*], Siddhanath Abasaheb Howal[2], Ganpati Martand Kharmate[3], Mahadeo Ramchandra Jadhav[4], Vikram Uttam Pandit[5]
[1*]Professor, Chemistry Department, Bharati Vidyapeeth college of Engineering, Navi Mumbai, India, Email: jjkadam702@gmail.com
[2]Assistant Professor, Gharada Institute of Technology, A/P Lavel, khed, Ratnagiri, Maharashtra, India, Email: siddhu.howal@gmail.com
[3]Assistant Professor, Physics Department, Bharati Vidyapeeth college of Engineering, Navi Mumbai, India, Email: ganpati.kharmate@bvcoenm.edu.in
[4]Assistant Professor, Chemistry Department, Bharati Vidyapeeth college of Engineering, Navi Mumbai, India, Email: mahadeojadhav2013@gmail.com
[5]Assistant Professor, Haribhai V. Desai College, Pune-411002, Maharashtra, India, Email:vikramupandit@gmail.com

Abstract: In the situation of Coronavirus disease 2019 (COVID-19), forecasting disease progression and identifying therapeutic drug targets is critical, especially given the nonattendance of a viable approach for treating severe cases. The preparation cohort revealed promising biomarkers, which were then precisely measured and employed to assess prediction accuracy across validation cohorts. This approach holds significant potential in enhancing understanding of severe COVID-19 and aiding the development of effective treatments. However, ultrasound-guided MRI (US-MRI) is an emerging modality that can noninvasively acquire multi-parametric information on COVID-19 and function without the need for contrast agents. This shows that neural network analysis of US-MRI transports exclusive prognosis data and this significantly improved prognosis performance. Consequently, the research proposed a deep neural network model of an Ensemble Multi-Relational Graph Neural Network (EMR-GNN) to determine the optimal model for predicting vascular biomarkers (CRP, IL-6, ferritin). In the nonappearance of a tailored treatment for this emerging virus, scientists are actively investigating various strategies to curb its replication. This work focuses on identifying potential drug targets, drawing from proteins abundant in lung material and those targeted by FDA-approved drugs as catalogued in HPA. This effort reflects a broader initiative within the methodical unrestricted to develop effective means of limiting virus replication. Accordingly, recognized five lung-improved proteins, comprising MRC1, SG3A1, CCL18, histone H4, and CLEC3B, were annotated as “drug targets”. For this, the researcher proposes a Heterogeneous Graph Structural Attention Neural Network (HGS-ANN) model to learn topological information of composite molecules and a Dilated Causal CNN-LSTM model with U-Net layers for modelling spatial-sequential information in Simplified Molecular-Input Line-Entry System (SMILES) sequences of drug data. The COVID-19 datasets are downloaded from the GEO database. These data are evaluated using Matlab software. The proposed work evaluated that the AUC of the work is 0.995, however, the AUC is measured based on sex, age, and chronic diseases. This model has a 0.933 accuracy in the subgroup of slices thicker than 1mm. However, the AUC curve and the classification outcome of the proposed method are compared with the existing rad model, deeper, and KNN models. In comparison to existing methods, the proposed model demonstrates superior performance. This research not only identifies potential therapeutic targets nonetheless also serves to uncover biomarkers crucial for comprehending the pathogenesis of undecorated COVID-19.

Keywords: Ultrasound-Guided MRI, COVID-19, Ensemble Multi-Relational Graph Neural Network, Heterogeneous Graph Structural Attention Neural Network, SMILES, and Food and Drug Administration.

1. INTRODUCTION

COVID-19 is an extremely communicable virus disease, first detected in December 2019. People affected by this disease will be affected by slight to unembellished breathing problems. It spread very rapidly, so it was announced as a pandemic. Constructed on clinical symptoms and associated medical investigations, COVID-19 patients are divided into four groups: severely severe, moderate, severe, and mild [1]. Clinicians would be healthier and able to handle the clinical therapy options if they could diagnose patients with poor prognoses early. The term "biomarker" refers to a class of biomolecules that serve as biological indicators of the existence, severity, or kind of a disease. They serve as important predictors of illness severity and diagnosis [2]. Risk factors of COVID-19 are older age, comorbidities chronic lung disease, hypertension, male sex, diabetes and cancer [3]. For the organization of patients based on their condition, primarily the identification of biomarkers is required [4]. Recently utilized COVID diagnosis methods are nuclear acid amplification test, serological test, imaging, biosensors, and microfluidic approach [5]. Artificial intelligence (AI) algorithms, especially deep learning, and neural networks have uncountable progress in the image-recognition field. They are suitable for identifying complex configurations in imaging information and providing valuations of radiographic appearances [6]. Imaging characteristics, particularly those of CT scans, can reveal pleural alterations, bronchial abnormalities, and lung parenchyma [7].

International Journal on Recent and Innovation Trends in Computing and Communication
ISSN: 2321-8169 Volume: 11 Issue: 9
***Article Received:** 25 July 2023 **Revised:** 12 September 2023 **Accepted:** 30 September 2023*

Examples of very important biometrics include coughs and sounds from the trachea, oesophagus, and thoracic cavity [8]. These data have the potential to measure droplet/aerosol production and, consequently, disease transmission related to coughing and other expiratory events, in addition to patient condition. The findings offer recommendations for patient care, early disease identification, and disease management, with a focus on COVID-19 [9]. After the disease is diagnosed, the appropriate response is "treatment with the correct drug at the correct amount of dose to the right patient" [10]. Although the right drug is applied to fight against coronavirus it will also have some risks called lateral effects. Presently using corona medicines has secondary effects such as depression, insomnia, irritability, anxiety, psychosis, aggression and confusion [11]. For disease identification and risk classification, mpMRI accompaniments normal clinical exams, systematic biopsies, and PSA measurements [12]. Cough is a potentially important biomarker. mpMRI is a vital new tool that can detect diseases [13]. With the help of multiparametric MRI, can diagnose haemosiderosis, hepatic fibrosis, and steatosis. It is an important step towards another way of liver biopsy [14]. For the development of the correct methodology, multiparametric analysis through variable digital biomarkers and alternative metrics relevant to the disease are exploited [15]. Challenges arise when custom this type of technology and maintaining simplicity while using the system. The prognosis for the disease is still bad; the 5-year survival rate across all disease phases is believed to be between 10% and 20%, and for individuals who have been diagnosed with a remote disease, it is 3%. This research contributes to the expenditure of mpMRI to overcome the challenges appearing in the identification of COVID-19. The motivation of this research is to use multiparametric monitoring of diseases with the least burden, through predictable and unpredictable symptoms of health conditions respectively [16]. The balance of the work is structured as follows: Section 2 depicts the literature survey of the research, and Section 3 exhibits the problem definition and the work's motivation. The planned research approach is revealed in section 4, the experimental and results conversation are made available in section 5, and the work's conclusion is shown in section 6.

2. Literature Survey

Chan *et al* [17] proposed that COVID-19 has enhanced the adoption of mpMRI, for reducing the requirement for a prostate biopsy, and the spread rate of COVID-19 can be condensed. When employed in conjunction with PSA density, mpMRI could decrease the number of pointless biopsies performed on patients who have a low likelihood of having clinically relevant PCa. Patients with results of Prostate Imaging-Reporting and Data System (PI-RADS) of less than 3 and Prostate Specific Antigen density of less than 0.15 ng/ml/ml are considered low-risk and safe to undergo supervision without MRI-targeted biopsy.

Non-invasive mpMRI was utilized by B Eicherbom *et al* [18] to examine the effects of severe COVID-19 on renal blood flow, tissue features, and oxygenation in recuperating patients. When compared to the same patients without AKI at follow-up five months following intensive care, severely COVID-19-recovered patients with high-grade AKI demonstrate decreased cortical and medullary ADC along with decreased total renal blood flow. However, no alterations in oxygenation for renal were evident in this situation.

Jurgen J. Futterer *et al* [19] optional that mpMRI can identify significant PCa for all biopsy conditions. The negative prognostic value of mpMRI plays a key role in identifying significant diseases. Prostate mpMRI can be also utilized to prevent significant diseases. Electrochemical biosensors for sensing multiparametric biomarkers at various molecular heights were discussed by Viviana Vasquez *et al* [20] besides their capacity to explain a person's health status. To preserve consistency and show their efficacy in comparison to the present standard of care, regulatory bodies need to compare and test the validity of various detection platforms. This is just one of many jobs that still need to be completed.

For COVID-19 patients, frontline healthcare professionals, and other high-risk individuals, Xiaoyue Ni *et al* [21] developed an automated remote control device and a statistical technique that overwhelms these restrictions. The findings present a wide range of data-merging alternatives for precision healthcare, including nevertheless not limited to COVID-19. Large volumes of available biometric data will be made available in appreciation of the scaled setup, which will serve as the foundation for prognostic illness replicas and patient care that is both efficient and affordable.

Multi-organ MRI assessment, according to Nichol Eichert *et al* [22], can enhance the current evaluation of multi-system anomalies in a diversity of illness conditions and provide information for earlier interventions and treatments. In both patient groups, there was a significant incidence of organ abnormalities, including steatosis (high-fat deposition) in the liver, pancreas, and kidney. Compared to 23% in long-term COVID-19, 35% of T2D patients had anomalies that were clustered and involved at least 2 organs. According to Jiantio Pu *et al* [23], expert or automated interpretation of CT scans is relatively less capable of differentiating between COVID-19 and CAP patients. The ability to precisely identify a substantial subset of non-COVID-19 situations, however, makes computerised image analysis appropriate for decision-making. Only 2% of COVID-19 patients were identified by this methodology, compared to 8–50% of CAP patients.

In COVID-19 patients, Maxwell *et al* [24] revealed the distinctive impacts of this virus and its disastrous significance on various organ systems. The laboratory analysis of precise strictures and the custom of proper monitoring of biomarkers gives clinicians the aptitude to brand proper medical verdicts and lead treatment for patients. Roland Derwand *et al* [25] described the results of COVID-19 patients in the casualty after initial treatment with low-dose HCQ, azithromycin and zinc (triple therapy) reliant on risk stratification. Risk classification and analysis-based action of COVID-19 casualties using triple therapy were accompanied by apparently fewer hospitalisations.

J Wang *et al* [26] proposed that a Chest CT scan is the most delicate imaging technology in the initial analysis and supervision of predicted and disease-confirmed COVID–19. Other imaging techniques utilized in the medical industry could also be applied in evaluating disease progression and observing critically ill patients with COVID-19 [27]. After studying all the literature, to overcome this problem the key objective of this research is to propose a DNN model for identifying vascular biomarkers, and prospective drug targets using electrochemical

International Journal on Recent and Innovation Trends in Computing and Communication
ISSN: 2321-8169 Volume: 11 Issue: 9
***Article Received:** 25 July 2023 **Revised:** 12 September 2023 **Accepted:** 30 September 2023*

biosensors to track several molecular stages of multipara metric biomarkers [28].

3. Research Problem Definition And Motivation

COVID-19, also known as SARS-CoV-2, stands as a novel respiratory virus that has brought about a profound impact on humanity [29]. At its genetic core, it features a single-strand positive-sense RNA virus structure. Notably, it belongs to the beta-type Coronavirus category, marked by distinct structural characteristics and binding mechanisms compared to other coronaviruses [30]. The virus testing landscape poses challenges, partly due to the limited availability of at-home detection options. This scarcity hampers the capturing of intricate health data, thus affecting the accuracy of analysis [31]. The three primary types of tests exploited for detecting biomarkers encompass viral, antigen, and antibody tests. Strong metrics for disease tracking and early identification obligations be established, requiring the synchronisation of multiple digital biomarkers and novel metrics relevant to the condition [32]. Overcoming these multifaceted requirements while maintaining user-friendly simplicity is pivotal for large-scale deployment in remote and continuous monitoring settings [33].

In the realm of COVID-19 detection and risk classification, multiparametric magnetic resonance imaging (mpMRI) has emerged as a game-changer [34]. While the markers might lack specificity, markers like acute-phase reactants, including ferritin, C-reactive protein (CRP), serum amyloid A (SAA), and procalcitonin, have proven sensitive indicators of serious COVID-19 illness [35-37]. Severe disease and susceptibility to rapid progression, including sepsis, are associated with raised white blood cell count, significant lymphopenia, reduced CD4, CD3, or CD8 T-lymphocyte counts, high neutrophil count, thrombocytopenia, and notably increased inflammatory biomarkers. This multiparametric approach facilitates monitoring with minimal imposition by encompassing conventional and unconventional health status markers. Notably, even cough, a superficially common occurrence, can potentially serve as an essential biomarker, complementing traditional vital signal analyses. The prognosis for COVID-19 remains challenging, with a 5-year survival rate estimated between 10% and 20% across all stages and a mere 3% for those diagnosed with distant disease. Given this scenario, there's a pressing need for more operative therapeutic approaches that extend survival and enhance patients' quality of life. This calls for comprehensive interventions that address both the economic and healthcare burdens posed by this virus [38-39].

4. Proposed Research Methodology

Numerous studies have been conducted throughout the COVID-19 pandemic to assess various immune system components to find predictive biomarkers of the illness. The purpose of this investigation was to assess a comprehensive multiparametric antibody panel comprising cellular and humoral components of the innate and adaptive immune response in patients with ongoing SARS-CoV-2 infection [40-44]. The potential of electrochemical biosensors to monitor multipara metric biomarkers at various molecular planes and their ability to provide a personalised assessment of a person's health condition is discussed in this article [45-48]. To categorise the sample constructed on the longitudinal development of several vital symbols and laboratory tests, the cluster analysis method was shaped. Three clusters were exploited to achieve the optimal clustering [49-53].

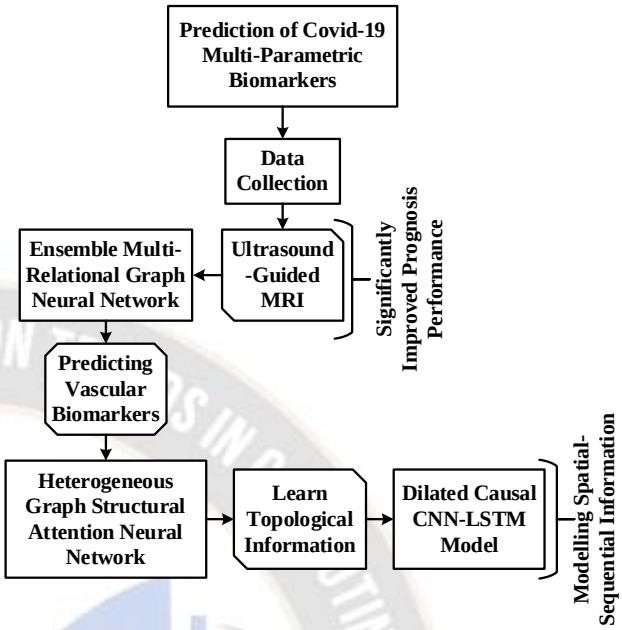

Figure 1. Block Diagram of the Proposed Method

Figure 1 shows the proposed project's block diagram. Referrals to homes accounted for 78.5% of medical discharges, whereas 6.2% of hospitalisations were due to referrals to other facilities and 11.5% of individuals were hospitalised due to death [54-56]. At hospitalisation, the patients' CCIs were on average 3.6. When the patients were categorised by CCI with a cut-off of 3 points, as was expected, those above the cutoff were older, demonstrated worse health status regarding hospitalisation features and higher death, and experienced a greater number of comorbidities such as cardiovascular events, liver conditions, diabetes, and cancer. However, a significant association with gender, age, and chronic disease were observed [57-59].

A. MR Imaging

The MRI scans were carried out for the Prodrome cohorts and Active Surveillance using a 3T machine (General Electric Healthcare, Discovery MR750, Chicago, IL, USA), following the PI-RADS v2 recommendations. A 32-channel pelvic phased-array coil with a resolution of 0.371 0.371 3.3 mm3 was applied to collect the T2-weighted imaging (T2w) diffusion-weighted imaging (DWI, b-values 50, 400, and 800). Scanner software was utilized to generate apparent-diffusion-coefficient (ADC) maps. A prostate MRI expert with more than 6 years of experience, an ultrasound-guided MRI (US-MRI), evaluated all MR pictures. The T2w images were utilized to identify and outline specific lesions having a PI-RADS score of 3.

1. Ultrasound-Guided MRI (US-MRI)

Targeted biopsies were carried out using the MRI and ultrasound guided-fusion technique (UroStation, Koelis, France) under ultrasound guidance. A LOGIQ E10 ultrasound machine (GE Healthcare) was employed to measure UGAP.

International Journal on Recent and Innovation Trends in Computing and Communication
ISSN: 2321-8169 Volume: 11 Issue: 9
***Article Received:** 25 July 2023 **Revised:** 12 September 2023 **Accepted:** 30 September 2023*

Each measurement was carried out on a patient within three months of the MRI-PDFF. Constructed on the descriptions on the T2w images with biopsy-proven considerable PCa (ISUP grade 2), binary masks were twisted for each patient for investigations. Every patient's DWIs with ADC standards were rigorously and painstakingly co-registered to their T2w pictures. Additionally, the 3D pictures were cropped to have dimensions of 128 x 192 x 24 voxels in the x, y, and z axes, covering the entire prostate area of interest.

B. Prediction of Vascular Biomarkers

When RA patients were compared to healthy controls, a biomarker of CV risk that is connected to both inflammation and thrombosis was found in the RA patients. Levels of biomarkers in circulation were assessed at baseline and following therapy in this post hoc investigation. In this study, an EMR-GNN model is presented for predicting vascular biomarkers. At one or two post-baseline time intervals through week 24, biomarkers were retrospectively evaluated (except for CRP) (Table S1). Timepoints were selected for the study based on prior results after sarilumab treatment or literature suggesting either acute or latent effects of RA medication on particular markers. The correlation between safety metrics and biomarkers was not assessed in this investigation.

1. Ensemble Multi-Relational GNN

Presenting EMR-GNN with the EnMP (collaborative message passing) layer now. Custom architecture that is decoupled, where the message transmission layer and the feature transformation are independent. Figure 2 depicts the whole framework, and the forward propagation procedure is as follows:

$$Y_{\text{pre}} = g_\theta \left(EnMP^{(K)}(f(X;W), R, \lambda_1, \lambda_2) \right) \quad (1)$$

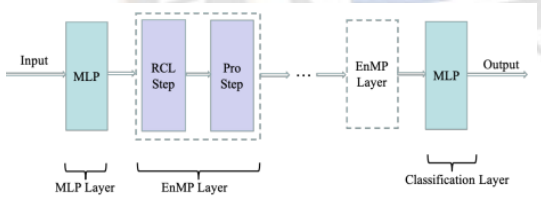

Figure 2. Model Architecture

Where X is the input feature for the nodes, and $f(X;W)$ stands for the MLPs or linear layers applied for feature extraction that is parameterized by W.$EnMP^{(K)}$, where R is the number of dealings and λ_1, $\lambda_2$are the hyperparameters of the message-passing layer, representing this proposed cooperative relational message-passing layer with K layers. MLPs acting as classifiers with learnable parameters θ are represented $g_\theta(\cdot)$. The training damage is given as $l(W,\theta)D\ y*i, y\hat{}i$ where $y*i$ and $y\hat{}i$ are the predicted and ground-truth labels of node I, respectively, and D is a discriminator function of cross-entropy. The parameters in EnMP layers are optimised during forward propagation while the parameters in MLPs, namely W and, are optimised in a backpropagation way. Can see that the EMR-GNN is based on a distinct optimisation objective. Additionally, EMR-GNN has several two benefits:

- It was determined that the EnMP can preserve the original data of the nodes with a teleport (or restart) probability, reducing over-smoothing.
- In the conventional RGCN, a parameterized relation encoder or relation-specific weight matrix is employed for each relation. The over-parameterization issue is significantly mitigated by EnMP, which associates a relation with a single learnable weight coefficient.

C. Drug Testing

Vero E6 cells were employed for all drug screening procedures. One day preceding to infection, cells were seeded in opaque 96-well plates. In either DMSO, water, or methanol, drug stocks were formed. Using an 8-point 1:2 dilution series, the drugs were thinned from stock to 50 μM. Before infection at MOI 0.01 or 0.004, cells were pre-treated for 2 hours (h) with the medication at 37°C/5% CO_2. Every plate had a vehicle control, and each screen had each treatment carried out three times. Parallel plates were not infected to observe the cytotoxicity of the medication alone in addition to the infected plates. This configuration produced three independent screens. According to the manufacturer's instructions (Promega), cells were cultured for 3 days at 37º C with 5% CO_2. A plate reader called the Molecular Devices Spectramax L was utilized to extend the luminescence. Benztropine mesylate, Fluphenazine dihydrochloride, amodiaquine dihydrochloride dihydrate, amodiaquine hydrochloride, thiethylperazine maleate, trimaran, mefloquine hydrochloride, anisomycin, terconazole veteran, fluspirilene, clomipramine hydrochloride, hydroxychloroquine sulphate, promethazine hydrochloride, emetine dihydrochloride hydrate and chloroquine phosphate were all purchased from Sigma. The following medications were bought from Fisher Scientific: gemcitabine hydrochloride, toremifene citrate, imatinib mesylate, chlorpromazine hydrochloride, and toremifene citrate.

1. Heterogeneous Graph Structural Attention Neural Network

Innovative embedding techniques are utilized to gather additional contextual information for both pharmaceuticals and protein sequences, and the HGSA architecture is implemented to learn the organizational data of the medication.

Effectively using molecular structure data to highlight the connections between atoms in the drug is a crucial indicator for the calculation of DTA. To do this, utilized RDKit1 to modify the SMILES chemical compounds molecular graph representation $G = (V, E)$, where each node represents the chemical bond between the i-th and j-th atoms and $e_{ij} \in E$ is denoted by $v_i \in V$ for the i-th atom. Numerous research studies have demonstrated the superiority of graph attention networks (GAT) in modelling graph representation. However, due to the complexity of the HR, where every two objects (nodes) are linked via various semantic information paths, which are known as meta-paths, it can be seen that the correlation concerning nodes in the generated compounds' HG can have different semantics reflected in meta-paths. For standard GAT only performs attention at the node level and is unable to make customs of meta-path semantic relations, it is ineffective for handling such heterogeneous molecular networks. Therefore, when embedding the system into a low-dimensional space, it cannot preserve the graph meta-path architectural information;

International Journal on Recent and Innovation Trends in Computing and Communication
ISSN: 2321-8169 Volume: 11 Issue: 9
***Article Received:** 25 July 2023 **Revised:** 12 September 2023 **Accepted:** 30 September 2023*

consequently, the learned embedding could be used for other downstream errands.

To do this, present hierarchical attention schemes, in which first perform attention at the node level to learn the weights of neighbours N^{Φ} of meta-path Φ, and then combine them to acquire the embedding of the semantic-specific node. These schemes are inspired by the heterogeneous graph attention network. The best-weighted combination of the semantic-level node embedding for the targeted task is then found by computing the difference between meta-paths using semantic-level attention.

Any kind of node has unique feature spaces as a result of node heterogeneity. Therefore, compute the node-type transformation matrix M_{Φ_i} as specified in equation (2) for projecting characteristics of each kind of node into the same feature space.

$$h_i' = M_{\Phi_i}.h_i \quad (2)$$

Where i stands for node type and h_i' and h_i reflect the node's original and projected features, respectively. To capture the weights between node pairs (i,j) with meta-path, the self-attention method is then used. Accordingly, the node-level attention e_{ij}^{Φ} computed with equation (3), where att_{node} designates the neural network that implements the node-level attention, represents the comparative importance of node $j \in N_i^{\Phi}$ for the node, i. This attention was then normalised with the softmax gathering to obtain the weight coefficient $\propto_{ij}^{\Phi}$ which is formulated in equation (4)

$$e_{ij}^{\Phi} = att_{node}(h_i', h_j';\ \Phi) \quad (3)$$

$$\propto_{ij}^{\Phi} = softmax(e_{ij}^{\Phi}) \quad (4)$$

The projected features of the neighbours can then be merged with the appropriate coefficients to generate the embedding (meta-path) that corresponds to the node i as shown in equation (5).

$$Z_i^{\Phi} = \sigma \sum_{j \in N_i^{\Phi}} \propto_{ij}^{\Phi}.h_j' \quad (5)$$

Where Z_i^{Φ} stands for the node that i discovered to be embedded on the meta-path Φ through its neighbours. However, just one meta-path is applied to regulate the attention weight, or $\propto_{ij}^{\Phi}$, such attention only picks up on certain types of semantic information. Additionally, see that the high variability of graph data is brought on by the scale-free character of HGs. To solve this issue and maintain the stability of the method of training, multi-head attention should be added to node-level attention. The learned implanting is shared to produce the semantic-specific embedding as stated in equation (6) by applying the node-level attention w to K times.

$$Z_i^{\Phi} = \|_{k=1}^{K} \sigma\left(\sum_{j \in N_i^{\Phi}} \alpha_{ij}^{\Phi}.h_j'\right) \quad (6)$$

Where, || denotes concatenation, and $Z = \{Z\Phi_0, Z\Phi_1, \cdots, Z\Phi_P\}$ represents grouped semantic embedding generated from node-level attention on the P meta-path set $\{\Phi_0, \Phi_1, \ldots, \Phi_P\}$.

In general, each node in the graph contains a variability of semantic data types and semantic-specific node embedding that each corresponds to a particular feature of node t. The semantics of many meta-paths essential also be combined to achieve collective learning of node embedding. Semantic-level attention is used to discourse this challenge since it can recognise the significance of different meta-paths and make customs of them for the intended activity. When P sets produced by node attention are input, the learned weights of each meta-path $\{\beta\Phi_0, \beta\Phi_1, \ldots, \beta\Phi_P\}$ can be expressed with equation (7),

$$\{\beta\Phi_0, \beta\Phi_1, \ldots, \beta\Phi_P\} = att_{sem}\{Z\Phi_0, Z\Phi_1, \ldots, Z\Phi_P\} \quad (7)$$

Measure the similarity between the altered embedding and vector q of semantic-level attention after applying a nonlinear transformation to the semantic-level embedding to ascertain its relevance. As shown in equation (8), also determine the significance of each meta-path as the regular of all the semantic-specific node embedding. Equation (9) is then used to normalise the results to provide the value $\beta\Phi_i$ which Φ_i denotes the meta-path's influence on the molecular graph. Greater relevance is indicated by a greater value for $\beta\Phi_i$.

$$w\Phi_i = \frac{1}{|v|}\sum_{iev} q^T.tanh(W.Z_i^{\Phi} + b) \quad (8)$$

$$\beta\Phi_i = \frac{exp(w\Phi_i)}{\sum_i^P exp(w\Phi_i)} \quad (9)$$

Then, utilising the aforementioned semantic-specific embeddings can determine the final embedding Z by using the calculated weights as a parameter, as indicated in equation (10)

$$Z = \sum_i^P (\beta\Phi_i.Z_i^{\Phi}) \quad (10)$$

Sequential Learning

The chemical structure of drug compounds is depicted in this section using SMILES, which uses a line notation of atoms and covalent bonds. For instance, "CC1=C2C=C (C=CC...") is the arrangement of atoms and covalent bonds is designated. To be taught by later deep learning layers, the resulting SMILES sequence needs to be encoded. For SMILES tokens, one-hot encoding has been used in several research, nonetheless, this encoding technique ignores the contextual significance of the symbols and is unable to reveal the operability of the tokens in the surrounding context. To solve this problem, utilized Smi2Ve, a process similar to Word2Vec, to encrypt the tokens in the SMILES sequences. In which fixed-length SMILES symbols separate into a separate atom that is mapped by locating matching embeddings from the previously trained dictionary or by providing a random value if no embedding exists. To generate the final embedding matrix, atom embedding vectors are combined.

2. Dilated Causal Convolution-LSTM

The benefits of convolutions can be obtained by combining the widened and fundamental convolution, which makes use of both the qualities of causality and dilation simultaneously. An updated CNN model, which is regarded as a statistical model, was fashioned using dilated causal convolution (DCC). The system's memory isn't completely used up by the new architecture. The restricted spreading of the output sequence $y_1, y_2, \cdots, y_T$ Given the input sequence $x_1, x_2, \cdots, x_T$ is given as the product of the provisional probabilities calculated by equation (11), where N is the length of the amenable field.

$$p(y|x) = \prod_{i=1}^{T} P(y_i|x_{i-N+1}, -x_{i-N+2}, \ldots, x_i) \quad (11)$$

A Temporal Convolutional Network (TCN) for STLF is the most well-known DL design that makes an expenditure of DCC. The various blocks of the expanded fundamental convolutional filter used by TCN have kernel sizes of two or higher. Additionally, TCN uses a dilated causal filter that has more than three separate blocks of stacked layers. The output and input sizes of the TCN architecture are made to be the same as the dilated fundamental layer by implementing zero padding. In the various blocks of the expanded contributing convolutional

International Journal on Recent and Innovation Trends in Computing and Communication
ISSN: 2321-8169 Volume: 11 Issue: 9
***Article Received:** 25 July 2023 **Revised:** 12 September 2023 **Accepted:** 30 September 2023*

filter, the TCN network's dilation factor is 1, 3, 4, 12, and 24, correspondingly.

Residual U-Net Architecture

The capacity to exploit low-level features while preserving high-level semantic information is the main characteristic of U-net architecture. The concept behind U-net is analogous to that of residual networks. To establish a communication link between low- and high-level convolution layers in U-net, low-level features are replicated to their corresponding high-level features. This technique facilitates the training of deep learning models and permits the backpropagation of errors between layers. Some academics have planned a hybrid model that uses residual blocks in place of the U-net's plain convolution layers to combine the ideas of residual networks and the U-net.

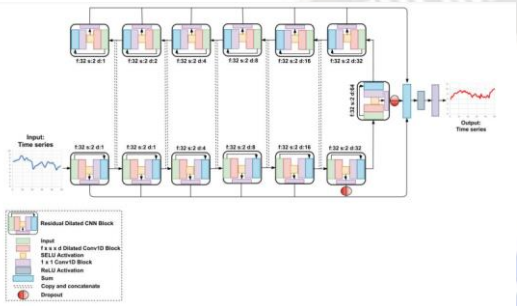

Figure 3. Residual U-Net (ResUnet) Architecture

In this study, a ResUnet architecture made up of the leftover SeriesNet building components is examined. Figure 3 illustrates to application of the bottom six residual blocks like SeriesNet before using the seventh block the one with the greatest dilation rate as a bridge to transmit data to the upper six residual blocks. The architecture had a rising number of dilation units the largest enlargement stretched a worth of 64 steps and applied a diminishing number of dilations to the remainder blocks. It resembled an encoder-decoder network. The amount of leftover blocks both before and following the bridge remained constant. The bottom residual blocks' matching top residual blocks received long skipped connections from the bottom remaining blocks. Top-level residual blocks were able to recover or improve the chronological information lost to dilation by copying and concatenating the output of bottom blocks with the input of top blocks with the same amount of dilations. Comparable to SeriesNet, made the final prediction by activating ReLU after summing the bounced influences of each remaining block. To lessen the impact of previous trends, failure was employed at the missed link of the sixth outstanding block. The output steps were equivalent to the input steps when using the 11 convolution layer with a linear activation at the output layer, which allowed for direct prediction.

3. Screening FDA- Appropriate Compounds for Anti-SARS-CoV-2 Movement

The 290 FDA-approved drugs were subjected to a thorough medication screening to find any that would be effective in contradiction of MERS-CoV and SARS-CoV (6). With the introduction of SARS-CoV-2, prioritised challenging 20 of the 27 hits for antiviral activity against the novel virus. These hits were found to constrain both of the before-verified coronaviruses. The screening began at 50 M and included an 8-point, 1:2 dilution sequence with infections carried out at multiplicities of infection (MOI) of either 0.01 or 0.004. Three days after infection (dpi), CellTiter-Glo (CTG) tests were conducted to compare the relative vitality of drug-treated cells to vehicle control-treated cells. The cytotoxicity of the medication alone was evaluated in uninfected samples. The relative luminescence data from the CTG assay allowed for the calculation and plotting of the percent inhibition (of virally-induced cell death) and the percent cytotoxicity of the medication alone.

Drug Screen Validation

To validate the compound screening process for identifying potential antiviral agents, opted to focus on a subset of drugs. Among these, Chloroquine (CQ) has garnered significant attention as a prospective COVID-19 treatment (12). Consequently, conducted a more in-depth investigation into hydroxychloroquine (HCQ) and CQ, both of which were part of the initial screening (Table 1). To proceed, cells of Vero E6 were cultured and subjected to a 2-hour pre-treatment with the selected drug before being exposed to SARS-CoV-2 infection at a MOI of 0.1. After 24 hours, the culture supernatant was collected to determine the virus titer through a TCID50 assay, while the cells were harvested in TRIzol for assessment of viral mRNA production. The administration of both drugs led to a substantial reduction in viral mRNA levels, particularly at higher concentrations, without inducing any adverse drug-related effects. This reduction was notably observed in both RNA-dependent RNA polymerase (RdRp) and nucleoprotein (N) mRNA expression levels across the concentration spectrum. Furthermore, the impact of the treatment extended to viral replication, as evidenced by an important decrease in SARS-CoV-2 production. HCQ exhibited greater sensitivity in inhibiting SARS-CoV-2 production compared to CQ, aligning with its lower IC50 value in the cell viability assessment. To delve deeper, conducted a time-of-addition assay with the highest HCQ concentration to understand its mode of action. Intriguingly, introducing HCQ at 2 hours post-infection (HPI) resulted in some inhibition, albeit not complete. This suggests that HCQ might influence other periods of the biological life cycle beyond the entry stag

Potential Therapeutic Drug Target Discovery against SARS-CoV-2 Infection

Exploring the potential for therapeutic intervention, the investigation focuses on the interplay between SARS-CoV-2 infection and the host, with a spotlight on amino acids, proteome, and lipidome profiles in plasma. These profiles offer promising avenues for identifying therapeutic drug targets, as they mirror the dynamic virus-host interaction. By delving into lung tissue-enriched proteins and FDA-approved drug targets catalogued in HPA, a study has pinpointed five lung-enhanced proteins MRC1, histone H4, CLEC3B, SG3A1, and CCL18 – all deemed potential "drug targets." Notably, MRC1 (CD206) emerges as a significant player, serving as a pivotal C-type lectin receptor found on M2 macrophages and utilized as a defining surface marker for this macrophage subset. MRC1 also promotes immunotolerance and has anti-inflammatory properties. A chemokine called CCL18 (AMAC1, MIP4) draws

International Journal on Recent and Innovation Trends in Computing and Communication
ISSN: 2321-8169 Volume: 11 Issue: 9
***Article Received:** 25 July 2023 **Revised:** 12 September 2023 **Accepted:** 30 September 2023*

lymphocytes like CD8 + and CD4+ T cells, which may be involved in cellular and humoral immune responses. A prior investigation revealed that either immunological dysregulation or macrophage activation syndrome was present in all COVID-19 patients with undecorated breathing failure. For patients with severe COVID-19, regulating macrophage activation may be a possible treatment approach. It was also recommended that MRC1 be considered as a potential therapeutic candidate for the dealing of COVID-19. MRC1 is the target of metformin, which has been licenced to decrease the M2-like polarisation of macrophages.

5. Experimentation And Result Discussion

Datasets related to COVID-19 were downloaded after the Gene Expression Omnibus (GEO) database. Select GSE150819 and GSE147507 for analysis based on the screening criterion "COVID-19 OR SARS-CoV-2, Homo sapiens". To study the unembellished acute respirational syndrome coronavirus 2 (SARS-CoV-2), human bronchial organoids (HBO) from commercially available cryopreserved primary human bronchial epithelial cells (hBEpC) were formed in GSE150819. This selected three SARS-CoV-2-infected samples and three control samples for analysis. Primary human lung epithelial cells (NHBE) and lung adenocarcinoma cells (A549, Calu-3) from GSE147507 were preferred for the study and mock-treated or SARS-CoV-2-infected.

Table 1. Simulation System Configuration

Simulation System Configuration	
MATLAB	Version R2021a
Operation System	Windows 10 Home
Memory Capacity	6GB DDR3
Processor	Intel Core i5 @ 3.5GHz
Simulation Time	10.190 seconds

Table 1 depicts the simulation system configuration for the proposed work. The suggested method is then assessed and placed to the test using the Matlab R2021a programme. The proposed work runs on Windows 10 Home and has 6GB of DDR3 RAM. The simulation duration for the job is 10.190 seconds, and it also uses an Intel Core i5 @ 3.5GHz processor.

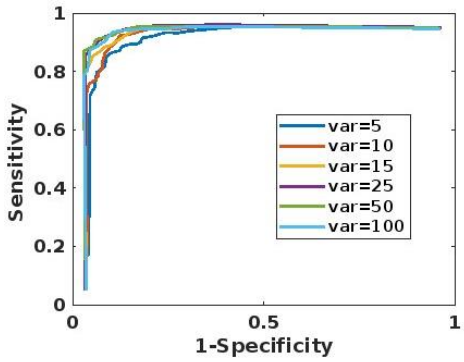

Figure 4. ROC Curve Analysis

Figure 4 shows the ROC curve analysis for the ability to combine multiple omics signatures elected using the random forest to distinguish between the non-severe and the severe group. Based on the proteome, amino acid, and lipidome data for the exercise cohort, constructed an accidental forest machine learning model, with 25 significant variables including 4 proteins and 21 lipids preferentially preferred. In the training set, this model's AUC was 0.995, with a 95% confidence interval of 0.957-1, and all samples could be categorised into the appropriate category.

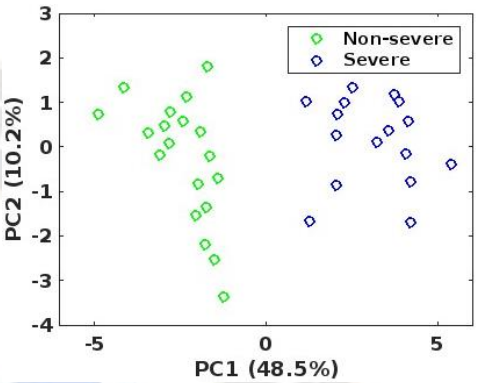

Figure 5. Principle Component Analysis for the Severe Groups and Non-Severe

Utilizing a principle component analysis, the study successfully differentiated samples into distinct groups based on 25 molecular panels. The grouping accuracy is illustrated in Figure 5. The classification relied on specific molecular signatures, including essential ceramides (Cer), glycosylceramides (CerG), cholesterol ester (ChE), phosphocholines (PC), phosphatidylethanolamines (PE), phosphatidylinositol (PI), triacylglycerides (TG), and proteins (CLEC3B, GELS, CAMP, GGH). Of notable significance were ceramides such as Cer (d18:2/22:0), Cer (d18:1/24:0), Cer (d22:0/O-18:0), CerG2GNAc1 (d36:1) and Cer (d24:0/O-18:0), in addition to glycosylceramides including, CerG2 (d18:2/16:0), and CerG1 (d18:2/24:0). Additionally, the presence of ChE (18:1), various phosphocholines, phosphatidylethanolamines, phosphatidylinositol, triacylglycerides, and the proteins CLEC3B, GELS, CAMP, and GGH played a critical role in the classification process. Remarkably, CLEC3B emerged as a particularly enriched protein with prognostic implications and potential diagnostic, associated with the pulmonary immune microenvironment. This integrated molecular analysis holds promise for advancing diagnostic precision and understanding the intricate molecular underpinnings in relevant contexts.

International Journal on Recent and Innovation Trends in Computing and Communication
ISSN: 2321-8169 Volume: 11 Issue: 9
***Article Received:** 25 July 2023 **Revised:** 12 September 2023 **Accepted:** 30 September 2023*

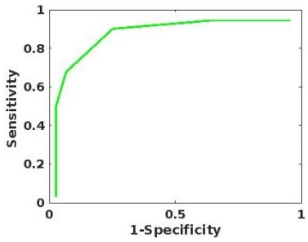

(a) ROC Curve Analysis

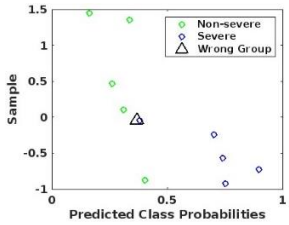

(b) Performance of the Model in Ten COVID-19 Patients

Figure 6. Validation Performance in Validation Cohort 1

To verify the exactness of these 25 molecular signs in plasma selected as potential markers to distinguish between severe and non-severe patients, their profusions in fresh plasma samples from a separate cohort of ten patients were investigated. Figure 6(a) illustrates the ROC analysis was used to evaluate the prediction. Using these 25 molecules, the AUC could achieve 0.991 with a 95% CI of 0.75-1. As seen in figure 6(b), one patient was incorrectly assigned to a group. Clinical retrospective research revealed that this patient's condition did not worsen after being admitted to the intensive care unit; instead, they just needed non-invasive ventilation (other severely ill patients required invasive breathing). Investigated other public datasets to evaluate the presentation of the biomarker panels identified in this work. Comparatively to earlier studies, adopted significantly complemented approaches in this investigation, enriching more small proteins and favouring more lipid types. Successful in locating several brand-new, previously unreported COVID-19 molecular markers. So, the only dataset identified that might be used for validation is the one. With the help of this information, were able to measure 19 molecules out of the 25 chemical signatures, with an AUC of 0.901 (95% CI: 0.807-0.973) used to categorise the non-severe n as 54 from the severe group. According to these findings, the independent cohort study's performance appears to be generally well-received.

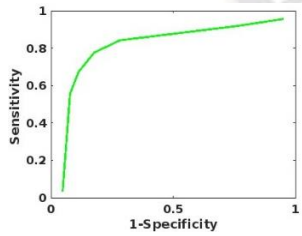

(a) ROC Curve Analysis

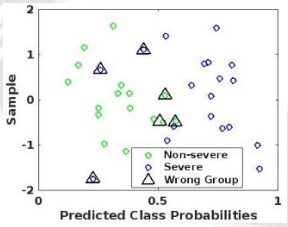

(b) Predicted Class Probabilities

Figure 7. Validation Performance in Validation Cohort 2

The potential predictive power of these compounds in urine was also examined in addition to plasma validation, as urine samples were obtained noninvasively and also represented dynamic changes in disease. For some lipids that were not secreted in urine or their abundance was below the technique detection threshold, eight molecules could finally be identified in urine samples. The ROC analysis was used to assess the prediction. Figure 7(a) showed that the AUC with 95% CI (0.7-1) could reach 0.912. The incorrectly assigned samples were highlighted in figure 7(b). Three serial samplings were performed over the whole admission on one patient to get three severe samples that were identified as belonging to the non-severe group. Two serial samplings were performed over the whole admission on two patients to obtain three non-severe samples that were categorised as severe. Overall, the accurate urine prediction demonstrated the viability of patient dynamic monitoring.

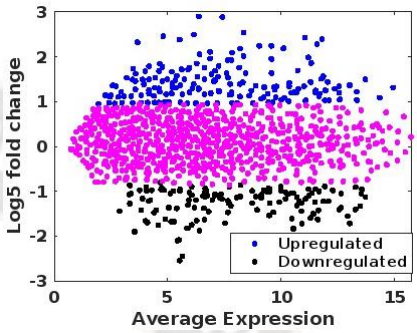

Figure 8: Volcano Plot of Counted Proteins in COVID-19

Investigated the differential expression of proteins in COVID-19 vs. healthy, non-severe vs. healthy, severe vs. healthy, and severe vs. non-severe groups. In total, 1254 proteins were measured in the samples. Figure 8's volcano plots showed that 118 dysregulated proteins (32 downregulated and 86 upregulated) were found between the COVID-19 (severe and non-severe) and healthy group, 104 proteins (76 upregulated and 28 downregulated), 143 proteins (80 upregulated and 63 downregulated), and 105 proteins (34 upregulated and 71 downregulated) between the severe and non-severe groups.

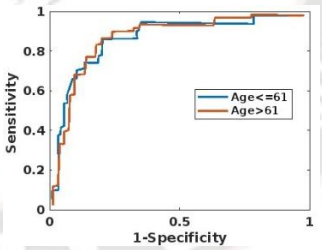

(a) Age

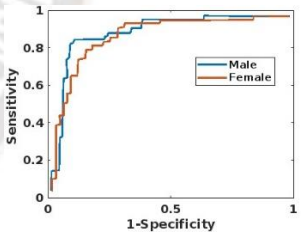

(b) Sex

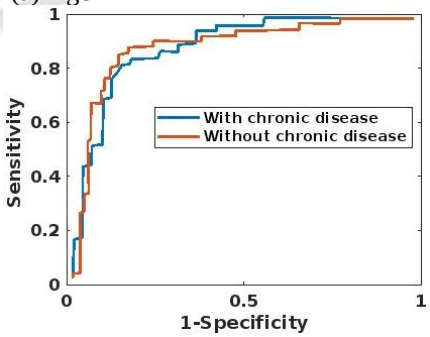

(c) Chronic Diseases

Figure 9. Area under Curve the Receiver Operating Characteristic Curve

International Journal on Recent and Innovation Trends in Computing and Communication
ISSN: 2321-8169 Volume: 11 Issue: 9
***Article Received:** 25 July 2023 **Revised:** 12 September 2023 **Accepted:** 30 September 2023*

Figure 9 shows that it performs age, sex, and chronic disease-specific stratified analysis on all patients. The middle age of all patients (61 years) served as the cut-off for age segmentation. Diabetes, hypertension, and chronic pulmonary illness all fall under the category of chronic diseases. The findings demonstrated that the combined model performed admirably in all circumstances and that it was unaffected by age ($P = 0.95$ by Delong test (DT), sex ($P = 0.63$ by DT), or chronic diseases ($P = 0.13$ by DT). Additionally, this model's accuracy is 0.856 in the subgroup of slices with a thickness under 1 mm and 0.933 in the subgroup of slices with a thickness over 1 mm.

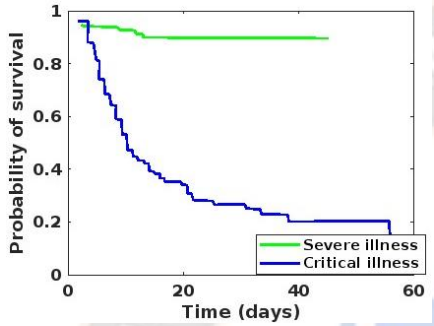

Figure 10. Kaplan–Meier Curves of Severe and Critical Cases

Figure 10 shows the Kaplan-Meier survival curve based on the combined model, stratified by severity grade, and compared using two-sided log-rank testing. In addition, Supplementary 5 displays the Kaplan-Meier survival curves for the Rad and DL models. The combined model outperforms the Rad and DL replicas in footings of stratification, according to the results. Notably, it was discovered that there was a considerable alteration between the outcomes of the combined model for severe and critical illness severities ($P < 0.001$).

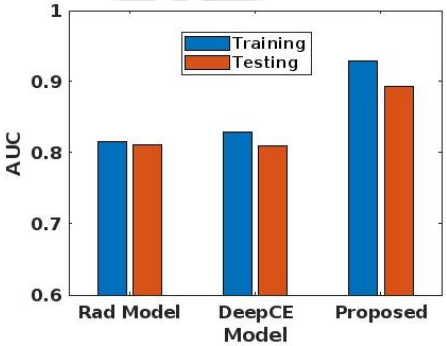

Figure 11. Performance of the Developed Models in the Training and Test Cohorts

The presentation of the developed models in training and testing cohorts is presented in figure 11. In the 5-fold cross-validation experiments, the mean AUC of the merged model was found to be 0.855 (range: 0.827–0.932) and RSD=3.81 in the test cohort, indicating satisfactory method robustness. Here, the rad model produces the AUC values of 0.827 for training and 0.824 for testing, and the DeepCE model produces the AUC values of 0.83 for training and 0.816. Meanwhile, the Rad model and deep CE model also show stable performance. However, the concert of the proposed model is significantly better than the other models ($P < 0.05$).

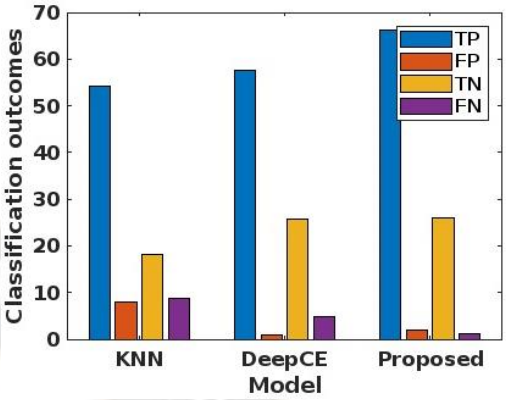

Figure 12. Classification Outcome of the Work

Figure 12 reveals the classification outcome of the proposed work compared with the KNN, and DeepCE models for false positive rate, true positive rate, false negative, and true negative. Compared to these existing methods, the proposed method produces a higher performance in that it produces higher values for a true positive rate of 67.5% and a true negative of 28%. However, it produces lower false positive and false negative rates at 3.5%, and 1.4%, respectively.

6. Research Conclusion

Worldwide fatality rates have substantially increased as a result of the novel coronavirus pneumonia (COVID-19)'s rapid dissemination. Despite many efforts, the speedy formation of an effective vaccine for this unique virus will take a lot of time and depends on the identification of drug-target (DT) interactions using commercially available drugs to uncover potential inhibitors. In this work, the US-MRI is an emerging modality that can noninvasively acquire multi-parametric information on COVID-19. An EMR-GNN is presented to determine the optimal model for predicting vascular biomarkers. However, an HGS-ANN method is introduced to learn topological data about multiple particles. However, the dilated Causal CNN-LSTM model with U-Net layers for modelling spatial-sequential information in SMILES sequences of drug data. This work utilizes the GEO database to analyse the COVID data. The collected samples are performed using Matlab software. Through experimental research, putative biomarkers, including up-and down-regulated genes, were derived using statistical methods and a set-theory consensus approach. The correctness of the suggested model was found to be higher than that of the other classifiers after training the machine learning models on various biomarker sets. On the complete dataset, a 5-fold cross-validation procedure to assess the robustness of the suggested technique. The entire dataset was specifically separated into five randomly generated folds, four of which were used for model training and one for model testing. Following five iterations of the training-testing procedures, the mean AUC was calculated. Conducted a stratified study that took into

consideration age, sex, and chronic disease to gauge the robustness of the model. The DT was utilized to associate the different ROCs' prediction capacities. Utilising comparable plasma and urine samples from the new COVID-19 patient cohort, the forecast supremacy was confirmed, with AUC reaching 0.991 and 0.912, respectively. The detected probability survival is $P < 0.001$, and the probability values for chronic diseases is $P = 0.13$ by using the DT. The proposed method compares the AUC, and classification outcome with the existing models like a rad model, DeepCE, and KNN models, while compared to these methods, the proposed method produces higher performance. The model's findings revealed a positive relationship between patient outcomes. The essence of the suggested approach is combining two separate feature types to produce a superior model, making it applicable to an assortment of additional classification tasks.

REFERENCES

[1] J. Cheng, X. Zhou, W. Feng, M. Jia, X. Zhang, T. An, M. Luan, Y. Pan, S. Zhang, Z. Zhou, and L. Wen, "Risk stratification by long non-coding RNAs profiling in COVID-19 patients," Journal of cellular and molecular medicine, vol. 25, no. 10, pp.4753-4764, 2021.

[2] H. Hampel, S. Lista, and Z.S. Khachaturian, "Development of biomarkers to chart all Alzheimer's disease stages: the royal road to cutting the therapeutic Gordian Knot," Alzheimer's & Dementia, vol. 8, no. 4, pp.312-336, 2012.

[3] T.P. Velavan, S.R. Pallerla, J. Rüter, Y. Augustin, P.G. Kremsner, S. Krishna, and C.G. Meyer, "Host genetic factors determining COVID-19 susceptibility and severity," EBioMedicine, vol. 72, pp.103629, 2021.

[4] S.A. Vajiha Begum, M. Pushpa Rani, "Recognition of neurodegenerative diseases with gait patterns using double feature extraction methods," IEEE - 2020 4th International Conference on Intelligent Computing and Control Systems (ICICCS), pp. 332-338, 2020, 10.1109/ICICCS48265.2020.9120920

[5] F.P. Caruso, G. Scala, L. Cerulo, and M. Ceccarelli, "A review of COVID-19 biomarkers and drug targets: resources and tools. Briefings in Bioinformatics," vol. 22, no. 2, pp.701-713, 2021.

[6] R. Maia, V. Carvalho, B. Faria, I. Miranda, S. Catarino, S. Teixeira, R. Lima, G. Minas, and J. Ribeiro, "Diagnosis methods for COVID-19: a systematic review," Micromachines, vol. 13, no. 8, pp.1349, 2022.

[7] A. Hosny, C. Parmar, J. Quackenbush, L.H. Schwartz, and H.J. Aerts, "Artificial intelligence in radiology," Nature Reviews Cancer, vol. 18, no. 8, pp.500-510, 2018.

[8] D. Dong, Z. Tang, S. Wang, H. Hui, L. Gong, Y. Lu, Z. Xue, H. Liao, F. Chen, F. Yang, and R. Jin, "The role of imaging in the detection and management of COVID-19: a review," IEEE reviews in biomedical engineering, vol. 14, pp.16-29, 2020.

[9] J. Rogers, X. Ni, W. Ouyang, H. Jeong, J.T. Kim, A. Tzavelis, A. Mirzazadeh, C. Wu, J.Y. Lee, M. Keller, and C. Mummidisetty, "Long-term, continuous, and multimodal monitoring of respiratory digital biomarkers via wireless epidermal mechano-acoustic sensing in clinical and home settings for COVID-19 patients," 2020.

[10] Athi sakthi, Pushpa Rani, "Detection of Movement Disorders Using Multi SVM," Global Journal of Computer Science and Technology, vol. 13, no.1, pp. 23-25, 2013.

[11] X. Ni, W. Ouyang, H. Jeong, J.T. Kim, A. Tzavelis, A. Mirzazadeh, C., Wu, J.Y., Lee, M., Keller, C.K. Mummidisetty, and M. Patel, "Automated, multiparametric monitoring of respiratory biomarkers and vital signs in clinical and home settings for COVID-19 patients," Proceedings of the National Academy of Sciences, vol. 118, no. 19, pp. e2026610118, 2021.

[12] T. Röddiger, C. Clarke, P. Breitling, T. Schneegans, H. Zhao, H. Gellersen, and M. Beigl, "Sensing with Earables: A Systematic Literature Review and Taxonomy of Phenomena," Proceedings of the ACM on Interactive, Mobile, Wearable and Ubiquitous Technologies, vol. 6, no. 3, pp.1-57, 2022.

[13] V. Vásquez, and J. Orozco, "Detection of COVID-19-related biomarkers by electrochemical biosensors and potential for diagnosis, prognosis, and prediction of the course of the disease in the context of personalized medicine," Analytical and Bioanalytical Chemistry, pp.1-29, 2022.

[14] A. Komathi, M. Pushpa Rani, "Trust performance of AODV, DSR and DSDV in wireless sensor networks," IEEE - Second International Conference on Current Trends In Engineering and Technology," pp. 423-425, 2014.

[15] N.M. Zadeh, N.S.M. Asl, K. Forouharnejad, K. Ghadimi, S. Parsa, S. Mohammadi, and A. Omidi, "Mechanism and adverse effects of COVID-19 drugs: a basic review," International Journal of Physiology, Pathophysiology and Pharmacology, vol. 13, no. 4, p.102, 2021.

[16] H.C. Demirel, and J.W. Davis, "Multiparametric magnetic resonance imaging: Overview of the technique, clinical applications in prostate biopsy and future directions," Turkish journal of urology, vol. 44, no. 2, pp.93, 2018.

[17] R. Mayer, B. Turkbey, P. Choyke, and C.B. Simone, "Combining and analyzing novel multi-parametric magnetic resonance imaging metrics for predicting Gleason score," Quantitative Imaging in Medicine and Surgery, vol. 12, no. 7, pp.3844, 2022.

[18] R. Banerjee, M. Pavlides, E.M. Tunnicliffe, S.K. Piechnik, N. Sarania, R. Philips, J.D. Collier, J.C. Booth, J.E. Schneider, L.M. Wang, and D.W. Delaney, "Multiparametric magnetic resonance for the non-invasive diagnosis of liver disease," Journal of hepatology, vol. 60, no. 1, pp.69-77, 2014.

[19] G.G. Chiddarwar, S.V. Balshetwar, B.P. Vasgi, "Blockchain based record date management system using artificial intelligence," Neuroquantology, vol. 20, no. 11, pp. 3847-3853, 2022.

[20] V.W.S. Chan, A. Asif, J.S.E. Koe, A. Ng, C.F. Ng, and J.Y.C. Teoh, "Implications and effects of COVID-19 on diagnosis and management of prostate cancer," Current Opinion in Urology, vol. 32, no. 3, pp.311-317, 2022.

[21] A. Komathi, M. Pushpa Rani, "Shift reduce parser based malicious sensor detection for predicting forest fire in WSNs," Wireless Personal Communications, vol. 103, pp. 2843-2861, 2018.

[22] P. Eckerbom, T. Luther, E. Cox, J. Weis, M. Hultström, M. Lipcsey, F. Palm, S. Francis, P. Liss, and R. Frithiof, "Reduced Renal Apparent Diffusion Coefficient at Follow Up after COVID-19 Associated Acute Kidney Injury," 2022.

[23] J.J. Fütterer, A. Briganti, P. De Visschere, M. Emberton, G. Giannarini, A. Kirkham, S.S. Taneja, H. Thoeny, G. Villeirs, and A. Villers, "Can clinically significant prostate cancer be detected with multiparametric magnetic resonance imaging? A systematic review of the literature," European urology, vol. 68, no. 6, pp.1045-1053, 2015.

[24] V. Vásquez, and J. Orozco, "Detection of COVID-19-related biomarkers by electrochemical biosensors and potential for diagnosis, prognosis, and prediction of the course of the disease in the context of personalized medicine," Analytical and Bioanalytical Chemistry, pp.1-29, 2022.

[25] X. Ni, W. Ouyang, H. Jeong, J.T. Kim, A. Tzavelis, A. Mirzazadeh, C. Wu, J.Y. Lee, M. Keller, C.K. Mummidisetty, and M. Patel, "Automated, multiparametric monitoring of respiratory biomarkers and vital signs in clinical and home settings for COVID-19 patients," Proceedings of the National Academy of Sciences, vol. 118, no. 19, pp. e2026610118, 2021.

[26] N. Eichert, A. Telford, A.D.R.I.A.N.A. Roca-Fernandez, A. Hamid, Thomaides-Brears, H.B. Dennis, A. Banerjee, R.S. Ali, G. Thanabalasingham, G. Kemp, And D. Cuthbertson,

"1166-P: Distinct Phenotypes of Multiorgan Abnormalities in Long COVID and Type 2 Diabetes Identified by Multiparametric Magnetic Resonance Imaging. Diabetes," 71(Supplement_1), 2022.

[27] J. Pu, J. Leader, A. Bandos, J. Shi, P. Du, J. Yu, B. Yang, S. Ke, Y. Guo, J.B. Field, and C. Fuhrman, "Any unique image biomarkers associated with COVID-19," European radiology, vol. 30, no. 11, pp.6221-6227, 2020.

[28] P. Brinda, M. Pushpa Rani, "Analysis of Early Leave Pest Detection," International Journal on Recent and Innovation Trends in Computing and Communication, vol. 4, no.5, pp. 2321-8169, 2016.

[29] M.D. Weidmann, K. Ofori, and A.J. Rai, "Laboratory biomarkers in the management of patients with COVID-19," American Journal of Clinical Pathology, vol. 155, no. 3, pp.333-342, 2021.

[30] R. Derwand, M. Scholz, and V. Zelenko, "COVID-19 outpatients: early risk-stratified treatment with zinc plus low-dose hydroxychloroquine and azithromycin: a retrospective case series study," International Journal of Antimicrobial Agents, vol. 56, no. 6, pp.106214, 2020.

[31] N. Islam, S. Ebrahimzadeh, J.P. Salameh, S. Kazi, N. Fabiano, L. Treanor, M. Absi, Z. Hallgrimson, M.M. Leeflang, L. Hooft, and C.B. van der Pol, "Thoracic imaging tests for the diagnosis of COVID-19," Cochrane Database of Systematic Reviews, vol. 3, 2021.

[32] Nihar Ranjan Kar, "Advancement Of Artificial Intelligence In Pharmacy: A Review," Shodhsamhita, vol. IX, no. (II(IV)), pp. 514-529, 2022.

[33] Nihar Ranjan Kar, "Osmotically Controlled Drug Delivery Systems: A Review," Indian Journal of Natural Sciences, vol. 13, no. 72, pp. 43372-43394, 2022.

[34] Nihar Ranjan Kar, "Nanotechnology-Based Targeted Drug Delivery Systems for Brain Tumors," Indian Journal of Natural Sciences, vol. 12, no. 68, 35081-35094, 2021.

[35] Nihar Ranjan Kar, "Liposomal Drug Delivery System: An Overview," Shodhasamhita: Journal of Fundamental & Comparative Research, vol. VIII, no. 5, pp. 123-134, 2022.

[36] Nihar Ranjan Kar, "A Review on Targeting of Drugs to Brain," Indian Journal of Natural Sciences, vol. 11, no. 64, pp. 2021.

[37] Nihar Ranjan Kar, "Niosomal Drug Delivery System: An Overview," Madhya Bharti, vol. 82, no. 14, pp. 180-190, 2022.

[38] Nihar Ranjan Kar, "Nutraceuticals in Pharmaceutical Field," Indian Journal of Natural Sciences, vol. 13, no. 72, pp. 43165-43171, 2022.

[39] Nihar Ranjan Kar, "Subas Chandra Dinda. Colon Specific Drug Delivery System: An Approach to Target Colonic Diseases," International Journal of Pharmaceutical Sciences and Research, vol. 10, no. 3, pp.1080-1088, 2019;

[40] Nihar Ranjan Kar, Subas Chandra Dinda, "Formulation and in vitro Characterization of Metronidazole Loaded Polymeric Microspheres for Colon Specific and Sustained Drug Delivery," Pharm Methods, vol. 10, no. 1, pp. 1-8, 2019;

[41] A.P. Senthil Kumar, S. Yuvaraj, S. Janaki, "Experimental investigations of Co3O4, SiO2, cotton seed oil additive blends in the diesel engine and optimization by ANN-SVM process," Journal of Ceramic Processing Research, vol. 21, no. 2, pp. 217-225, 2020.

[42] S. Yuvaraj, A.P. Senthil Kumar, M. Muthukumar, K. Sadesh, S. Janaki, "Certain studies on influence of nano catalysts Co3O4, SiO2 blended with CME-diesel in combustion," Materials Today: Proceedings, vol. 51, pp. 1612-1618, 2022.

[43] R.K. Pattanaik, S. Mishra, M. Siddique, T. Gopikrishna, S. Satapathy, "Breast Cancer Classification from Mammogram Images Using Extreme Learning Machine-Based DenseNet121 Model," Genetics Research, pp. 2731364, 2022.

[44] S.K. Mohapatra, S. Prasad, G.M. Habtemariam, M. Siddique, "Identify determinants of infant and child mortality based using machine learning: Case study on Ethiopia," Big Data Analytics and Machine Intelligence in Biomedical and Health Informatics: Concepts, Methodologies, Tools and Applications, pp. 21–45, 2022.

[45] Shiva Shankar Reddy, Gadiraju Mahesh. "Risk Assessment of Type 2 Diabetes Mellitus Prediction using an Improved Combination of NELM-PSO," EAI Endorsed Transactions on Scalable Information Systems, vol. 8, no. 32, 2021 May.

[46] Shiva Shankar Reddy, N. Mahesh Gadiraju, Meghana Preethi, V.V.R. Maheswara Rao, "A Novel Approach for Prediction of Gestational Diabetes based on Clinical Signs and Risk Factors," EAI Endorsed Transactions on Scalable Information Systems. Vol. 10, no. 3, pp. 2023, Jan.

[47] Shiva Shankar Reddy, Nilambar Sethi, R. Rajender, Gadiraju Mahesh, "Forecasting Diabetes Correlated Non-alcoholic Fatty Liver Disease by Exploiting Naïve Bayes Tree," EAI Endorsed Transactions on Scalable Information Systems, vol.10, no.1, pp. e2-, 2023.

[48] Shiva Shankar Reddy, Nilambar Sethi, R. Rajender, "Risk Assessment of Myocardial Infarction for Diabetics through Multi-Aspects Computing," EAI Endorsed Transactions on Pervasive Health and Technology, vol. 6, no. 24, pp. e3-, 2020 Dec.

[49] Shiva Shankar Reddy, Nilambar Sethi and R. Rajender. "Rigorous assessment of data mining algorithms in gestational diabetes mellitus prediction," International Journal of Knowledge-based and Intelligent Engineering Systems, vol.25, pp.369–383, 2021.

[50] Tarun Kumar Kotteda, Manoj Kumar, Pramod Kumar, Rama Bhadri Raju Chekuri, "Metal matrix nanocomposites: future scope in the fabrication and machining techniques," The International Journal of Advanced Manufacturing Technology, 2022. https://doi.org/10.1007/s00170-022-09847-0

[51] Tarun Kumar Kotteda, Rama Bhadri Raju Chekuri, Naga Raju, Prasada Raju Kantheti, S. Balakumar, "Analysis on Emissions and Performance of Ceramic Coated Diesel Engine Fueled with Novel Blends Using Artificial Intelligence," Advances in Materials Science and Engineering, 2021, https://doi.org/10.1155/2021/7954488

[52] M. Siddique, D. Panda, "Prediction of stock index of tata steel using hybrid machine learning based optimization techniques," International Journal of Recent Technology and Engineering, vol. 8, no. 2, pp. 3186–3193, 2019.

[53] M. Siddique, D. Panda, "A hybrid forecasting model for prediction of stock index of tata motors using principal component analysis, support vector regression and particle swarm optimization," International Journal of Engineering and Advanced Technology, vol. 9, no. 1, pp. 3032–3037, 2019.

[54] S. S. Reddy, N. Sethi, R. Rajender, & V.S.R. Vetukuri, "Non-invasive diagnosis of diabetes using chaotic features and genetic learning," In Third International Conference on Image Processing and Capsule Networks, pp. 161–170, 2022. Cham: Springer International Publishing.

[55] S. S. Reddy, L. Alluri, M. Gadiraju, & R. Devareddi, "Forecasting Diabetic Foot Ulcers Using Deep Learning Models," Proceedings of Third International Conference on Sustainable Expert Systems, pp 211–227, 2023.

[56] R. S. Shankar, D. R. Babu, K.V.S.S. Murthy, & V. Gupta, 'An approach for essay evaluation using system tools," 2017 International Conference on Innovative Research In Electrical Sciences (IICIRES). IEEE. 2017.

[57] R. Shiva Shankar, & D. Ravibabu, "Digital report grading using NLP feature selection," In Soft Computing in Data Analytics,615–623, 2019. Proceedings of International Conference on SCDA 2018.

[58] Reddy, Shiva Shankar, M. Gadiraju, & V.V.R. Maheswara Rao, "Analyzing student reviews on teacher performance using long short-term memory," In Innovative Data Communication Technologies and Application, pp. 539–553, 2022. Singapore: Springer Nature Singapore.

[59] N. Mary Peter, M. Pushpa Rani, "V2V communication and authentication: the internet of things vehicles (IoTV)," Wireless Personal Communications, vol.120, no.1, pp. 231-247, 2021.